Experimental study of time and frequency properties of collective nuclear excitations in a single crystal (gamma-ray resonance)

1989 J. Phys.: Condens. Matter 1 10563

(http://iopscience.iop.org/0953-8984/1/51/025)

J. Phys.: Condens. Matter 1 (1989) 10563–10584. Printed in the UK

Experimental study of time and frequency properties of collective nuclear excitations in a single crystal

Yu V Shvyd'ko and G V Smirnov
I V Kurchatov Institute of Atomic Energy, Moscow, 123182 USSR

Received 21 February 1989

Abstract. The angular dependences of the time and frequency parameters of a single-crystal collective nuclear resonance were studied in a unified series of measurements and compared with the resonance parameters of an isolated nucleus. It was shown that, when approaching the Bragg angle (θ_B), the coherent character of gamma radiation interaction with the nuclear system in a crystal causes drastic changes of collective resonance parameters. A sharp reduction of the nuclear system response time—from 230 ± 10 ns for an isolated nucleus to 40 ± 10 ns at the Bragg peak—takes place. The nuclear resonance width increases from $3.5\Gamma_0$ (Γ_0 is the natural width) to $20 \pm 0.5\Gamma_0$. The resonance energy changes non-monotonically with the angle of incidence of radiation on the crystal and deviates from the resonance energy of an isolated nucleus by $(2.0 \pm 0.5)\Gamma_0$ as a maximum. The excitation spectra of the collective nuclear gamma resonances have an asymmetrical shape. The sign of the asymmetry changes when crossing the Bragg angle position.

The properties of the collective nuclear excitations were analysed with the theory of Kagan, Afanas'ev and Perstnev, as well as with that of Kagan, Afanas'ev and Kohn.

1. Introduction

A nuclear target in Mössbauer spectroscopy is usually considered as a set of independent resonantly absorbing and scattering centres that are concentrated within a sample space. In terms of this assumption, the presence of other resonant nuclei in the near neighbourhood does not influence the state of each isolated nucleus nor its behaviour in the scattering process. The physical reasons for such an assumption are related to the fact that direct inter-nuclear interactions in the solid state are practically absent. In the independent-nuclei model, the resulting scattering cross section turns out to be merely the sum of resonant cross sections relating to all scattering centres (forward scattering is not meant here).

As a rule, the approximation considered is quite satisfactory for the description of real situations, but appears to be deficient in some cases. The fact is that in a system of identical nuclei, where gamma radiation can interact resonantly with any nucleus, the gamma-radiation field is common to all nuclei. Therefore, for this reason alone the nuclei cannot be regarded as totally independent. Under definite conditions, excited states can appear that represent a dynamically coupled system of radiation field and nuclear matrix. Hence, in the general case, a system of identical nuclei should be considered as a collective resonator.

The phase correlations of the excitation probability amplitudes turn out to be essential for the occurrence of collective effects in a system of nuclear resonators. As is known,

0953-8984/89/5110563 + 22 $02.50

the collective spontaneous emission effect exists in a system of radiators [1], provided that the field coherently affects the radiators. In the optical range, where the wavelength λ is considerably larger than the characteristic inter-atomic distance a, this condition is easily met. With such a close arrangement of radiators, the wave has almost the same phase for all of them. However, in the case of nuclear gamma radiation, the reverse relation is valid: $\lambda \leqslant a$. It seems that in such circumstances one can hardly expect collective effects due to possible violation of coherence conditions. But still, even in this case there exist situations in which collective effects are possible, as for example, in the interaction of radiation with nuclei in a single crystal. Within the crystal space the strict regularity in the arrangement of radiators is maintained; thus we can expect a correlation of the nuclear excitation phases at various centres [2–10].

Owing to the conservation of phase memory in gamma-radiation scattering from an isolated nucleus and to the strict correlation of scattering phases from various nuclei, a coherent coupling of nuclear excitations through the radiation field is established in a crystal. The excited state, where the gamma-radiation field and the nuclear matrix are dynamically coupled, will often be referred to as a nuclear gamma exciton or, simply, a gamma exciton†. It is important that the notion of collective excitation relates to the radiative decay channel only, since in the radiationless channel caused by the internal electron conversion process, the nucleus that has been excited could be distinguished after the scattering process.

The gamma exciton (as well as the excited state of an isolated nucleus) can be characterised by excitation energy, resonance width and lifetime. These parameters for a gamma exciton can differ drastically from those for an isolated nucleus. By changing the direction of a beam incident near the Bragg angle, one can vary within a wide range the dimensions of a nuclear ensemble that responds coherently to the excitation. Far from the Bragg angle, the incident radiation excites the nuclei coherently only in a very thin crystal surface layer, so that in this case the properties of the gamma exciton should be close to those of an isolated nucleus. The largest deviation from the resonant parameters of an isolated nucleus can be expected when the nuclear system is excited exactly at the Bragg angle, i.e. when the nuclear ensemble, responding coherently, reaches maximum dimensions.

The theory [2, 6, 10] has predicted that as a consequence of coherent effects, one must observe a broadening of the reflection spectral band in the vicinity of the Bragg angle and, also, the speed-up of emission of radiation at the decay of a nuclear excited state. The broadening of the spectral band and the speed-up of emission were related by the authors to shortening of the lifetime of collective excited states.

One must note, however, that not only the above-mentioned coherent effects but also resonant self-absorption of radiation in bulk samples [13, 14] can lead to reflection spectral band broadening and to emission speed-up (see also Appendix). The self-absorption makes observation of coherent effects in crystals with defects rather difficult.

In an early experimental study of the frequency properties of collective nuclear excitations [15] the enhancement of a radiative channel in resonant scattering has been detected, which manifested itself in considerable broadening of the reflection frequency band in a crystal in the close vicinity of the Bragg angle. Also, the reflection intensity maximum was shown to be shifted from the isolated-nucleus resonant energy position.

† There is a definite analogy with the other elementary excitation in the solid state—the light exciton (polariton) [11]. However, there is one principal difference in the collectivisation mechanism. In the latter case it is established not only through the radiation field, but mainly through the Coulomb interaction between the centres. It is essential also that in the case of a light exciton the relation $\lambda \gg a$ holds. It should be noted also that the 'nuclear-exciton' term, which was introduced earlier in [12] for designation of collective states similar to that considered here, does not reveal the crucial role of gamma radiation in the collectivisation of radiators in a crystal.

The first attempt to measure the time behaviour of the Bragg nuclear scattering of gamma radiation from a single crystal was undertaken in [16]. Coherent excitation of nuclei in $^{57}Fe_2O_3$ was obtained with a synchrotron radiation (SR) pulse. The authors of [16] have reported a speed-up of gamma-photon emission in the Bragg direction after the SR flash. Since the role of resonant self-absorption due to crystal defects was not determined in this experiment, it is not clear to what extent the reported speeded-up emission could really be caused by the coherent response of a nuclear system.

Comparative measurements of the time behaviour of coherent and incoherent gamma-photon scattering in one and the same nuclear system in a crystal have been carried out [17]. This enabled one to reveal directly the effect of decay speed-up of single-crystal collective nuclear excitations. Time measurements were performed using the magnetic resonance shutter technique [18]. In this experiment an incident beam was used whose divergence was wide compared to the reflection region of the crystal. Thus, the complete set of Bragg modes of collective excitations was formed and the integral effect over all incident angles was observed. The first measurements of angular-resolved time characteristics of single-crystal collective nuclear excitations were carried out in [19]. The response time as a function of the deviation from the Bragg position of incident radiation was measured. The experiment has clearly demonstrated the effect of the speed-up decay of the Bragg modes of collective nuclear excitations.

The measurements of the decay behaviour of a collective nuclear state in a $^{57}FeBO_3$ crystal, excited by a SR pulse at different positions around the Bragg angle, have been performed in [20], where a strong speed-up of the coherent decay was observed. Recently the full time evolution of the Bragg scattered radiation from $^{57}Fe_2O_3$, excited by SR, was measured with very small primary beam divergence [21]. The time dependences of the de-excitation processes from the crystals excited by SR were in both cases strongly modulated by quantum beats, exhibiting the interference of nuclear hyperfine transitions.

The main purpose of this paper was to observe simultaneously the evolution of both time and frequency parameters of gamma excitons selectively excited at different angles in the Bragg region. The measurements of time and frequency dependences for the same sample were carried out. The comparison of measured resonant parameters of gamma excitons with those of an isolated nucleus was performed. The experimental data have been compared with the results obtained from the theory of coherent interaction of gamma radiation with the nuclear system in a crystal [6, 10]. Different simplified theoretical models were analysed.

2. Experimental scheme, crystal samples and measurement procedure

To study the time and frequency properties of the Bragg modes of nuclear gamma excitons, one should provide selectivity of their excitation and also perform time and energy analyses of the scattering process.

The scheme of the experimental set-up is shown in figure 1. The 14.4 keV $^{57}Co(Cr)$ Mössbauer radiation source (4 mm diameter) was fixed on the transducer and placed inside the lead shield. The initial source activity was 1.25×10^{10} Bq. The initial linewidth of the source was $\Gamma_s' = 0.18$ mm s^{-1}. Ten months later at the final stage of the experiment the source line was broadened to $\Gamma_s = 0.23$ mm s^{-1}. The cross section of the beam coming out from the shield was confined to a diameter of 4 mm by a collimator. The radiation beam passed successively through a pair of $^{57}FeBO_3$ crystals, which constituted the

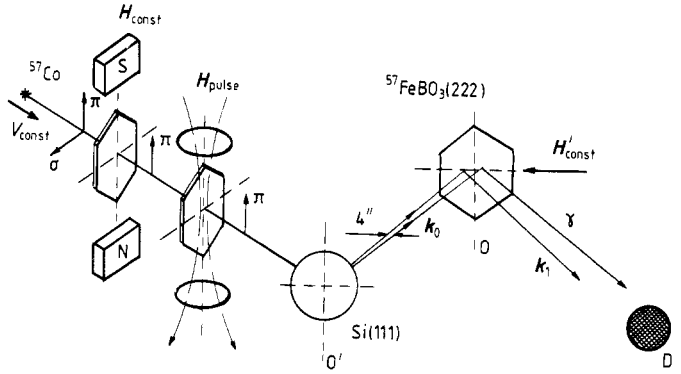

Figure 1. Scheme of the experimental set-up in a double-crystal geometry of coherent scattering: Si(1 1 1) × $^{57}FeBO_3$(2 2 2). In the gap between the Mössbauer ^{57}Co source and the Si crystal collimator the magnetic resonant shutter assembly is shown with two active elements—the $^{57}FeBO_3$ crystals. This assembly was installed for time dependence measurements only.

magnetic resonance shutter assembly. The first crystal was placed into a constant magnetic field $\boldsymbol{H}_{const}$, and the other one into a pulsed one $\boldsymbol{H}_{pulse}$. The shutter provided both polarisation and amplitude modulation of gamma radiation. A Si crystal was installed on the first axis of the goniometer-O′ and served as a collimator, providing gamma-beam divergence of 4″ after reflection from the (1 1 1) planes. The polarised, modulated and collimated beam was directed onto the $^{57}FeBO_3$ crystal under investigation.

2.1. Spectrometer and magnetic resonant shutter

The gamma photons, coherently scattered from the $^{57}FeBO_3$ crystal, were registered by a detector, D, installed in the scattering plane at angle $2\theta_B$ with respect to the direction $\boldsymbol{k}_0$ of the beam incident upon the crystal. A NaI(Tl) scintillation detector (diameter 10 mm × 0.1 mm) with ФЭУ-85 photomultiplier was used. It was placed at a distance of 25 cm from the crystal. Thus it recorded predominantly a diffracted coherent beam. The gamma-photon signals from the detector were processed by fast timing and slow energy analysis circuits. The energy resolution of the spectrometer was 25% for 14.4 keV gamma radiation, and the time resolution was 6 ns. A detailed description of the spectrometer network, similar to that applied in the present work, was given in [17, 18].

To study the time properties of nuclear excitations one should have a time reference. For this purpose a magnetic resonant shutter with $^{57}FeBO_3$ crystals as active elements was used here. A detailed description of its operation principle was given in [18]. The best mode of shutter operation was obtained when the gamma source was in resonance with the $^{57}FeBO_3$ crystals. Thus, the problem of resonant adjustment in both the shutter and the investigated nuclear system could be solved with a single transducer. The strongest modulation of a shutter was obtained at resonance with $\Delta m = 0$ transitions. For this reason all time measurements were performed with the radiation at resonance with this transition.

The shutter was placed in the gap between the gamma source and the Si crystal (see figure 1). It provided a fast uncovering of the gamma-ray beam in 10 ns [18] (figure 2). Some 720 ns later the shutter was closed. The beam chopping to the initial level (which existed for $t < 0$) lasted 25 ns. The time dependence of the gamma-radiation intensity at $t > 720$ ns has a rather complicated shape caused by the process of spontaneous demagnetisation of $FeBO_3$ crystals [18, 22]. The operation frequency of the shutter was 0.5 MHz.

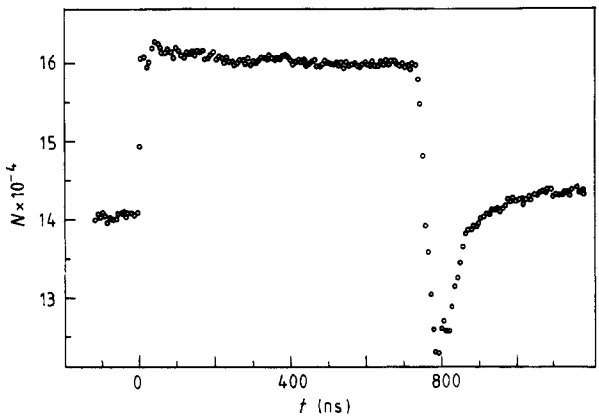

Figure 2. Time dependence of the Mössbauer radiation intensity passed through the magnetic resonant shutter. The zero time is marked at the moment when the shutter uncovers the radiation flux. (One channel is equal to 7 ns.)

The modulated gamma-radiation beam enabled us to measure the following: first, the time dependence and the characteristic response time τ_{ex}^{*} following the excitation of a nuclear system by the gamma-radiation step (after $t = 0$); and, secondly, the time dependence and the characteristic emission time τ_{ex} at coherent de-excitation of a nuclear system after chopping of the incident beam (at time $t = 720$ ns).

2.2. $^{57}FeBO_3$ crystal

A $^{57}FeBO_3$ crystal was used for the investigations, since it is close to ideal in its structural perfection [23]. The use of such a crystal was a necessary condition for maximum enhancement of coherent nuclear excitation effects in which we are interested. The isotropic enrichment in ^{57}Fe was 95%. The crystal's linear dimensions were 6×10 mm^2 and thickness $L = 0.05$ mm. Crystal planes (1 1 1) were parallel to the surface. The perfection of the single-crystal plate was studied by several methods.

First of all, an x-ray topogram was recorded using the Lang method (the spatial resolution was 1 μk). It has shown that both visible defects and macroscopic tensions are practically absent in the central part of the crystal. The topogram of the crystal under study was given earlier in [23, 24]. Data on crystal investigation by the Borrmann effect can be found there, also.

Furthermore, the quality of the $^{57}FeBO_3$ crystal was studied in a double-crystal Bragg diffraction $FeBO_3(4\,4\,4) \times {}^{57}FeBO_3(4\,4\,4)$ geometry using Cu K_{α_1} (8.05 keV) x-ray radiation. The width of an angular reflection curve of the crystal under investigation as $\Delta\theta_x = 7.0'' \pm 0.5''$ in such a geometry. The reflection coefficient was equal to $K_x = 0.51 \pm 0.01$, which is close to values calculated for a perfect crystal. The $\Delta\theta_x$ and K_x values were measured differentially over the crystal surface with an x-ray beam of small cross section: 0.2×4 mm^2. The error in $\Delta\theta_x$ and K_x corresponds to the spread in values obtained at different crystal points (except the edges—see below).

Finally, macroscopic crystal bending was measured in the described double-crystal diffraction geometry. For this purpose the relative angular positions of the rocking curve maximum at different crystal points were measured using a precision optical bench. It turned out that in the larger part of the sample the bending was lower than 2″. At the same time a small fraction of the crystal (edges) had a bending more than 5″. In order to

provide the necessary selectivity of gamma-exciton excitation, the bent edges were screened by a thin Cu foil fixed with wax on the crystal. The larger part of the crystal ($\xi = 0.76$, on account of foil shadow) was left open. After fixing the foil the sample was tested again to be sure that no additional bending was caused by the screening procedure.

After these tests the crystal was fixed on the second axis of a goniometer. It was oriented at angles close to $\theta_B = 10.29°$ with respect to a collimated gamma-ray beam reflected by Si(1 1 1) crystal. This θ_B value corresponds to the nearly pure nuclear Bragg reflection (2 2 2) in the $^{57}FeBO_3$ crystal [15, 17].

The $FeBO_3$ crystals belong to the class of canted antiferromagnets [25]. The magnetic moments of Fe atoms are located in the (1 1 1) plane of easy magnetisation. The Mössbauer spectrum of ^{57}Fe in the $FeBO_3$ crystals has a characteristic magnetic hyperfine splitting and consists of six lines [26]. A permanent magnetic field $\boldsymbol{H}'_{const} = 50$ A cm^{-1} was applied to the $^{57}FeBO_3$ crystal under investigation, which converted it into a single-domain state. The field was directed in the crystal plane (1 1 1) and, at the same time, in the scattering plane ($\boldsymbol{k}_0, \boldsymbol{k}_1$) (figure 1). The nuclear magnetic field was oriented perpendicular to the scattering plane. Under such conditions the π-polarised gamma-radiation component only interacted with nuclear $\Delta m = 0$ transitions, and the σ-polarised radiation only with $\Delta m = \pm 1$ transitions [15].

The Si and $^{57}FeBO_3$ crystals were adjusted in space so that the rotation axes O and O′ were perpendicular to the scattering plane to a good accuracy. For this purpose the angular rocking curves were taken in the Si(1 1 1) × $^{57}FeBO_3$ (2 2 2, $\Delta m = 0$) geometry with fine adjustment of the inclination of the $^{57}FeBO_3$ crystal with respect to a scattering plane. This fine adjustment was carried out until the narrowest rocking curve ($\Delta\theta_\gamma = 9.2''$) with the largest reflected intensity was obtained.

To show that the self-absorption effects due to structural defects can be neglected in the Bragg resonance scattering of gamma photons in a chosen crystal, we have measured the absolute reflectivity of the crystal and compared it with the theoretical value for an ideal sample. The value of the absolute reflectivity for gamma radiation was determined as $K_\gamma = (I_{out} - B)/(I_{in} - B)$. Here I_{in} is the resonant photon flux incident on a crystal, I_{out} is the reflected flux, and B is the background magnitude. In our case it was rather low: $B < 0.01$ count/s. The total intensity of gamma-photon flux reflected by the Si(1 1 1) crystal was $I' = 2.31 \pm 0.01$ count/s (on the day of measurement). Only a fraction of this flux hits the $^{57}FeBO_3$ crystal under investigation, installed in the Bragg reflection (2 2 2). The resonant part of this fraction was determined simply as $I_{in} = f_m \xi (I' - I'') = 0.77 \pm 0.03$ count/s, where f_m is the recoil-free fraction emitted by the source ($f_m = 0.73$) and $I'' = 0.92 + 0.05$ count/s is the intensity of gamma radiation passed by the crystal (the crystal itself was opaque for 14.4 keV radiation).

The reflected intensity at maximum was measured to be $I_{out} = 0.15 \pm 0.01$ count/s. Using these data one can obtain the reflectivity value $K_\gamma = 0.20 \pm 0.02$. In fact, K_γ should be even larger if one takes into account the role of different polarisations in the incident radiation. As has been mentioned, the $\Delta m = 0$ transition is excited by the π-polarised component only. The σ-polarised component is only scattered due to excitation of the wings of neighbouring $\Delta m = \pm 1$ resonances. The calculations (see details of similar calculations in § 4.1) have shown that under the given conditions the contribution of σ-polarised component to the scattered radiation intensity does not exceed 20%. Hence, the absolute reflectivity for an essentially π-polarised component is not less than 32%. This value is anomalously high, which shows the strong suppression of the inelastic incoherent scattering channels. A greater fraction of the collective nuclear excitation energy returns elastically into the radiative channel—at least six times larger than in

scattering from an isolated nucleus. The observed reflectivity $K_\gamma = 0.20 \pm 0.02$ is very close to that predicted by the theory for an ideal crystal. Using the divergence of the incident beam (4″) and bending of the crystal (2″), the theory yields $K'_\gamma = 0.22$. It will be recalled that an anomalously high reflectivity has also been observed in earlier measurements [27] using a similar crystal.

All preliminary measurements aimed at testing our crystal perfection assured us that the time and frequency characteristics we are going to determine in the Bragg scattering are just the nuclear gamma-exciton characteristics.

2.3. Selective excitation of the Bragg modes

Measurements of time or frequency properties of the Bragg modes of gamma excitons were carried out during a continuous angular scan of the $^{57}FeBO_3$ crystal in the region around the Bragg position. The effective counting rate of the Mössbauer photons reflected by the $^{57}FeBO_3$ crystal was only about 0.1 count/s. Thus, to obtain information with good statistical accuracy the measurements should be performed for a long time. In this case there exists a danger of slow uncontrolled temperature drifts of the relative angular setting of the $^{57}FeBO_3$ and Si crystals. To suppress the drifts temperature stabilisation was provided in a way similar to that in [28]. Also, the measurements were divided into rather short repeated cycles.

One measurement cycle lasted for 48 h. During this period the crystal was turned in the range $\theta_B - 10'' \rightarrow \theta_B + 10''$. The time dependences (or frequency spectra) of diffraction were recorded at the passage of each arcsecond. As a result of a 20″ turn, 20 time (frequency) dependences were recorded, each of them corresponding to the excitation of a different group of collective nuclear states. For good statistics the measurements were repeated and the data, corresponding to various cycles, were summed up. The position of the rocking curve maximum was used as a reference angular point for alignment of the time (frequency) dependences referring to the same angular range, but measured in different cycles. The rocking curves could be obtained easily in every cycle after summation of the information in each of 20 dependences. The widths of the rocking curves thus obtained in the measurement cycles differed slightly, but not by more than 1″ (at the average width of 9.5″). The total number of counts at the rocking curve peak was about 300 photons.

To stabilise the relative angular setting of the Si and $^{57}FeBO_3$ crystals within an arcsecond for at least 48 h, the goniometer with $^{57}FeBO_3$ and Si crystals was kept at constant temperature. For this reason it was put inside a plastic case where a constant temperature was maintained, slightly higher than room temperature. Temperature control was performed at one point not far from the $^{57}FeBO_3$ crystal. The accuracy of temperature stabilisation was ±0.1 °C.

As a result, the two-dimensional data file $T(t, \theta - \theta_B)$ was obtained in 50 cycles, which represents the intensity of coherently scattered gamma photons as a function of two parameters: t, the delay of gamma-photon emission from the crystal with respect to the zero time; and $\theta - \theta_B$, the deviation of the incident angle from the Bragg angle. In these measurements the gamma source was moving in a constant-velocity mode and was tuned to the transition with $\Delta m = 0$ in $^{57}FeBO_3$. In the same manner the two-dimensional data file $S(E_s, \theta - \theta_B)$ representing the intensity of coherent scattering as a function of energy, E_s, and the relative angle of gamma incidence, $\theta - \theta_B$, upon a crystal was obtained as a result of 20 measurement cycles. In this experiment the shutter had been removed from the beam and the source was moving in a constant-acceleration mode.

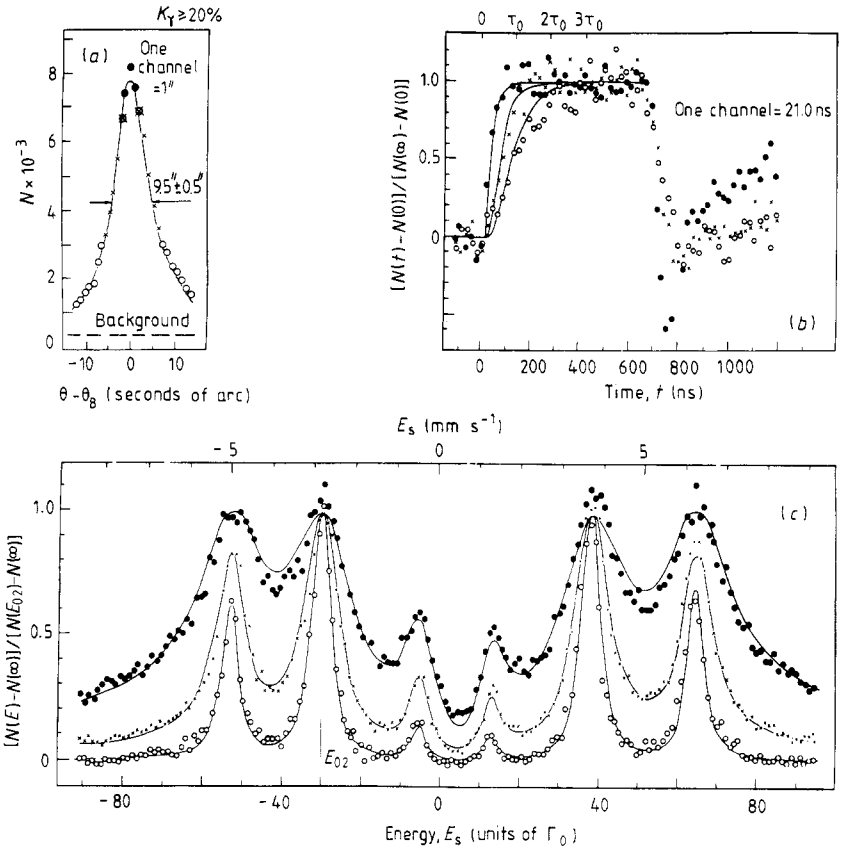

Figure 3. The intensity of the (222) nuclear Bragg reflection from the $^{57}FeBO_3$ crystal: an example of processing of the angular–differential time response $T(t, \theta - \theta_B)$ and the Mössbauer spectra $S(E_s, \theta - \theta_B)$. The collimation of the incident beam is 4″. (*a*) The rocking curve for $^{57}FeBO_3(222)$ at resonance with $\Delta m = 0$ (E_{02}), obtained from $T(t, \theta - \theta_B)$ after integration over t in the range 200 ns $< t <$ 700 ns. (*b*) The time response of a regular nuclear system in the $^{57}FeBO_3$ crystal following excitation by a nearly rectangular gamma pulse (figure 2) in different angular ranges near the Bragg position. (*c*) The Mössbauer diffraction spectra of $^{57}FeBO_3$ in the fixed angular intervals. Three angular intervals in the Bragg region were chosen: (●) the top of the Bragg maximum; (×) the slopes of the rocking curve; (○) the wings. Full curves: theoretical fit.

The measured $T(t, \theta - \theta_B)$ and $S(E_s, \theta - \theta_B)$ files contain information on time and frequency properties of different gamma-exciton Bragg modes.

3. The results of measurements

3.1. Time and frequency properties of gamma excitons

The two-dimensional data files $T(t, \theta - \theta_B)$ and $S(E_s, \theta - \theta_B)$ were used to plot frequency and time dependences of coherent scattering at the excitation of different gamma-exciton modes in the $^{57}FeBO_3(222)$ crystal. Let us denote by N the integrals of T and S taken in any angular or other intervals and assign them the meaning of intensity of coherent scattering. An example of the initial data processing of T and S files is given in figure 3.

Figure 3(*a*) shows the intensity of coherent resonant scattering as a function of the angular deviation from the Bragg position for gamma radiation at resonance with the $\Delta m = 0$ transition. It was obtained from $T(t, \theta - \theta_B)$ after summation over the time interval of 200 ns $< t <$ 700 ns. The curve width is equal to $9.5'' \pm 0.5''$. It is in good agreement with theoretical calculations, which are shown by the full curve (see § 4.2 for details). The same angular curve could be obtained from the $S(E_s, \theta - \theta_B)$ file with $E_s = E_{02}$.

To illustrate the angular-resolved time dependences of coherent scattering, three angular intervals have been chosen (figure 3(*a*)): the first, 7″ wide, on the wings of the rocking curve; the second, 4″ wide, on the slopes of the angular curve; and the third, 3″ wide, in the immediate neighbourhood of the Bragg angle. Figure 3(*b*) shows time dependences of coherent scattering in the selected angular intervals (the curves are normalised). Within the statistical accuracy achieved in the experiment, no differences in time dependences corresponding to symmetrical angular intervals were observed. This fact was used to improve the statistical accuracy. Time dependences given in figure 3(*b*) are the sums over symmetrical angular intervals. The full curves in figure 3(*b*) present the results of the theoretical calculations (see § 4.2).

As clearly seen, the response following the excitation is delayed. Let us determine the characteristic response time τ_{ex}^* as an interval between the zero time and the moment when the intensity of scattered gamma radiation reaches $1 - e^{-1} = 0.63$ of its maximal value. It can be seen from figure 3(*b*) that the delays differ depending on the Bragg mode excited. While approaching the Bragg angle the response time τ_{ex}^* is strongly speeded up.

When the gamma-photon flux is chopped at the moment $t = 720$ ns, the emission does not stop immediately, but proceeds for a characteristic time τ_{ex}. As is seen, a smaller value of τ_{ex}^* corresponds to a smaller emission time at spontaneous decay, τ_{ex}. The results of time measurements have been presented earlier in [19].

Figure 3(*c*) shows frequency dependences of coherent scattering corresponding to gamma-exciton excitation in the angular intervals selected. A drastic change in the response spectral band Γ_{ex} is observed when varying the angle of radiation incidence on the crystal (as usual, Γ_{ex} has been determined at the peak half-maximum).

It turned out that, contrary to the time dependences, there exists a substantial difference in frequency spectra measured in the angular intervals symmetrical with respect to the Bragg position. Figure 4(*a*) shows the spectra recorded in the regions 4″ wide with centres deflected by $\pm 3.5''$ from θ_B. First, a strong asymmetry of the spectral lines was observed. The sign of the asymmetry changes when crossing the Bragg angle. Secondly, the maximum of reflected intensity is reached not at the resonance energy of an isolated nucleus E_{02} (the broken lines in figure 4), but at the energy E_{ex}, which is either higher or lower than E_{02} depending on positive or negative deviation from the Bragg angle.

The data obtained in the measurements, $T(t, \theta - \theta_B)$ and $S(E_s, \theta - \theta_B)$, enable us to reveal the angular dependences of the gamma-exciton resonance characteristics: (i) the gamma-exciton response time $\tau_{ex}^*(\theta - \theta_B)$; (ii) the reflection spectral band width $\Gamma_{ex}(\theta - \theta_B)$; and (iii) the relative energy $E_{ex} - E_{02}$ at which the maximum of reflection intensity is reached. These dependences are shown in figure 5 and illustrate the most vivid time and frequency properties of gamma excitons. The full curves in figure 5 show the results of theoretical calculations using values from the experimental conditions. The broken curves in the same figure show theoretical curves for a hypothetical case when a plane wave of gamma radiation is incident on the crystal.

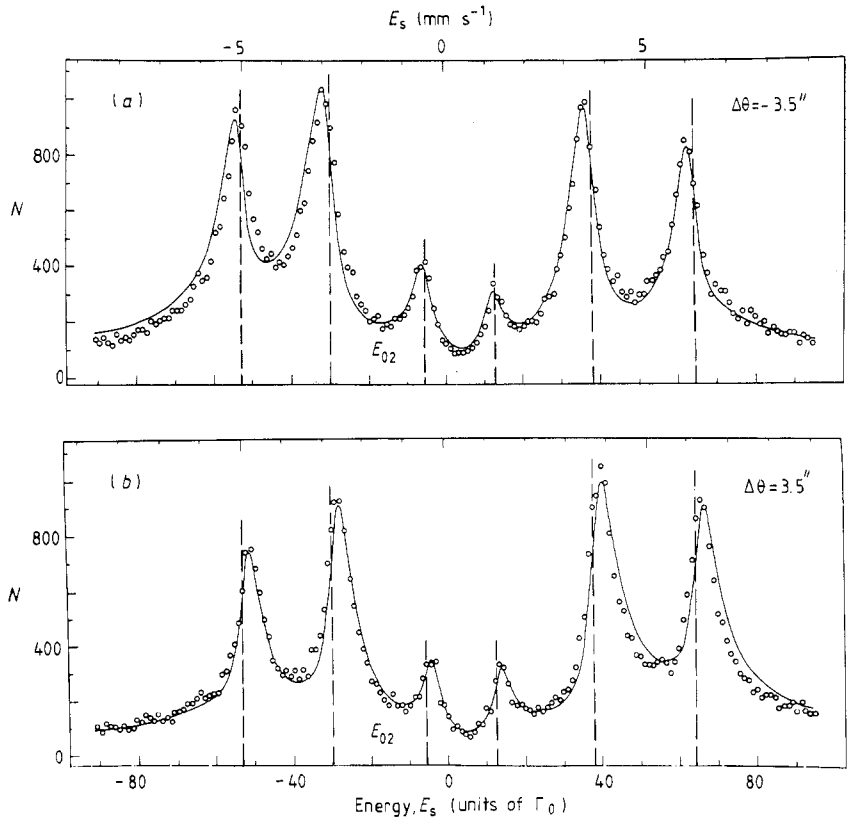

Figure 4. Mössbauer diffraction spectra measured in two symmetrical angular intervals about the Bragg position: (*a*) $-5.5'' < \theta - \theta_B < -1.5''$; (*b*) $1.5'' < \theta - \theta_B < 5.5''$.

3.2. Comparison with the resonant parameters of an isolated nucleus

The chain lines in figure 5 show the levels that correspond to the values of time and frequency parameters of an isolated nucleus. These data were obtained experimentally in the study of incoherent scattering of gamma rays in a crystal. In these experiments the conversion electrons were detected. The measurement technique and procedure are described in [29].

The response time of a nucleus excited at resonance by quasi-monochromatic radiation was measured to be $\tau_0^* = 230 \pm 10$ ns. In [29], τ_0^* was identified with the nuclear lifetime measured under conditions of excitation by quasi-monochromatic radiation. It exceeds the ^{57}Fe isomer proper lifetime $\tau_0 = 141.1$ ns inherent in spontaneous decay conditions.

As seen from figures 3(*b*) and 5(*a*) even at distance $+11.5''$ away from the Bragg angle, where the coherent scattering intensity is small (figure 3(*a*)), the characteristic response time of the nuclear system $\tau_{ex}^* = 170 \pm 30$ ns is less than the response time of an isolated nucleus $\tau_0^* = 230 \pm 10$ ns, though it does not differ much. When approaching the Bragg position the characteristic response time reduces strongly and in the close neighbourhood of the Bragg angle decreases down to the value of 40 ± 10 ns. Despite the limited angular resolution of the experiment ($4''$ is the beam divergence and $2''$ is the crystal bending), the response time of the nuclear system turned out to be six times

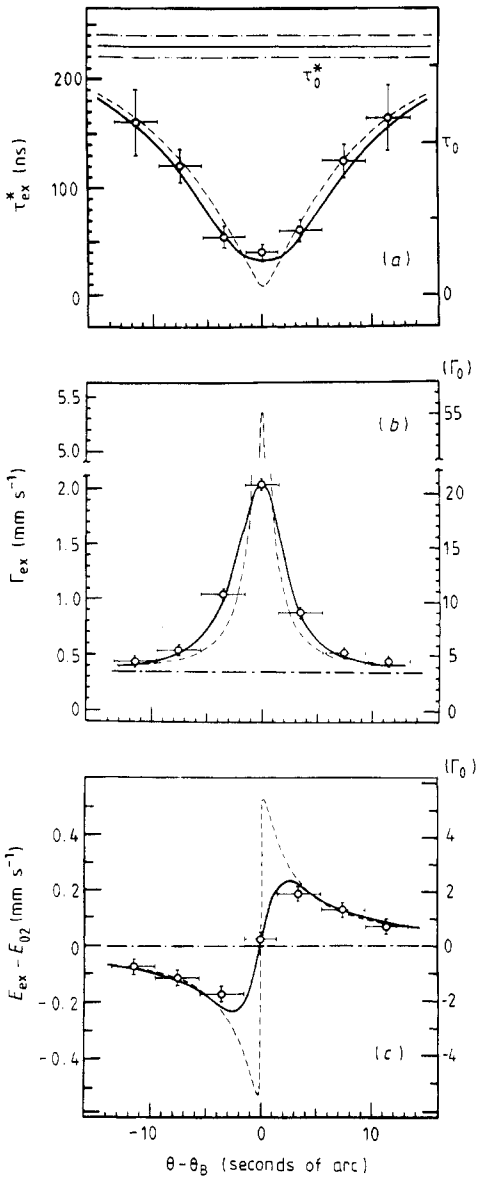

Figure 5. Angular-resolved time and frequency parameters of gamma excitons corresponding to the excitation of the $^{57}FeBO_3(222)$ crystal at resonance with $\Delta m = 0$ (full curves—theoretical fit): (*a*) gamma-exciton response time τ^*_{ex}; (*b*) width of the reflection spectral band Γ_{ex}; (*c*) E_{ex}, the energy at which the maximal probability of gamma-exciton excitation is reached (with respect to the excitation energy of an isolated nucleus E_{02}). The chain lines show the experimental resonance parameters obtained for an isolated nucleus. The broken curves show the calculation result for the case of an incident plane wave of radiation.

shorter than that of an isolated nucleus. As seen from figure 3(*b*), in the de-excitation after radiation chopping at the moment $t = 720$ ns the gamma-photon emission time also reduces when approaching the Bragg angle.

According to the energy–time uncertainty principle, the reduction of response time (or emission time) must be accompanied by the increase of reflection spectral band. As seen from figure 5(*b*), at distance $+11.5''$ away from the Bragg angle the nuclear system response takes place in an energy band slightly wider than the ordinary nuclear resonance width. However, when approaching the Bragg angle the reflection band width sharply increases and reaches the value of $20 \pm 0.5\Gamma_0$.

The observed angular dependence of frequency and time parameters of nuclear resonant Bragg scattering and their essential difference from similar scattering charac-

teristics for an isolated nucleus directly indicate the great significance of coherent radiative coupling of nuclear resonators in a crystal. This suggests the use of the nuclear gamma-exciton concept.

3.3. Principal results of the experiment

The data given in this section demonstrate the following fundamental properties of gamma excitons:

(i) The lifetime of a gamma exciton is less than that of an isolated nucleus and decreases when the Bragg position is approached.

(ii) The reflection spectral band of gamma excitons is broadened in the region around the Bragg angle.

(iii) The characteristic gamma-exciton energy differs from the resonance energy of an isolated nucleus.

(iv) The shape of a gamma-exciton spectral line is asymmetric; the asymmetry changes sign when crossing the Bragg angle position.

It will be recalled that the properties (ii) and (iii) have been observed initially in [15] (the asymmetry of the peak shape in the experimental spectra was not manifested due to scarce statistics). Property (i) was first demonstrated in [17, 19].

The gamma-exciton features outlined in this section will be discussed later in § 5. But let us first compare the present experimental data with the theory.

4. Comparison of experimental results with theory

4.1. Gamma-excitons spectra

To calculate the Mössbauer diffraction spectra in $^{57}FeBO_3(222)$, the following expression for the coherently scattered radiation amplitude in the Bragg geometry has been used [6]:

$$R^{s}(E,\alpha)=\frac{2g^{s}_{10}}{\alpha-2g_{00}\pm[(\alpha-2g_{00})^{2}-4g^{s}_{10}g^{s}_{01}]^{1/2}} \tag{4.1}$$

where

$$g^{s}_{km}=-\sum_{l=1}^{6}g_{0}(l)V^{s(l)}_{km}\frac{\Gamma_{0}/2}{E-E_{0l}+i\Gamma_{0}/2}+\chi^{s}_{km} \tag{4.2}$$

with

$$V^{s(l)}_{km}=\delta^{s,\pi}\delta_{\Delta m,0}+0.5\delta^{s,\sigma}\delta_{\Delta m,\pm1}[\cos(2\theta_{B})]^{|k-m|}. \tag{4.3}$$

The sign before the root was chosen so that $|R^{s}(E,\alpha)|\leq 1$. In (4.1) we have used the following notation: E is the gamma-radiation energy; the upper index s labels the eigenpolarisations of radiation (π, σ): $\alpha=-2\sin(2\theta_{B})\Delta\theta$; $\Delta\theta=\theta-\theta_{B}$ is the deviation from the Bragg angle; g_{00} and g^{s}_{01}, g^{s}_{10} are the scattering parameters in the equations of the dynamic theory of diffraction, which are proportional to the amplitudes of coherent scattering from a unit cell in the forward direction and at the Bragg angle, respectively. The sum in (4.2) is proportional to the coherent amplitude of nuclear resonant scattering from a $^{57}FeBO_3$ unit cell. Index l numbers all six hyperfine nuclear transitions in $^{57}FeBO_3$ with energies E_{0l}. $V^{s(l)}_{km}$ is the nuclear structural–polarisational tensor, which is expressed

by (4.3) in the case of (222) reflection. As seen from (4.3), the resonances with $\Delta m = 0$ ($l = 2, 5$) are excited by the π-polarised component of radiation only. The σ-polarised component excites the remaining resonances ($l = 1, 3, 4, 6$) with $\Delta m = \pm 1$. Equation (4.3) is valid only in the case when the magnetic field on the nuclei is perpendicular to the scattering plane, which corresponds to the experimental conditions.

The procedure of calculation of $g_0(l)$ for $^{57}FeBO_3$ was described in [15]. The values $g_0(l)$ thus obtained turned out to be larger than similar values given in [15], e.g. $g_0(2) = 3.23 \times 10^{-5}$. This is due to a higher isotropic enrichment in ^{57}Fe of the $^{57}FeBO_3$ crystal involved.

The scattering parameters (4.2) also contain the added quantities $\chi^s_{km} = (\chi^s_{km})' + i(\chi^s_{km})''$, which are proportional to the coherent amplitudes of electronic scattering from a crystal unit cell. For the (222) reflection in $^{57}FeBO_3$ the following values have been used here: $\chi'_{00} = -0.82 \times 10^{-5}$, $\chi''_{00} = 1.9 \times 10^{-7}$, $(\chi^\pi_{10})'' = 1.65 \times 10^{-7} = (\chi^\sigma_{01})'' \cos(2\theta_B)$ [15] and $(\chi^\pi_{01})' = 0.3 \times 10^{-7} = (\chi^\sigma_{01})' \cos(2\theta_B)$. It is seen that the largest Bragg electronic scattering parameter $(\chi^\pi_{01})''$ is two orders of magnitude smaller than the nuclear resonance ones.

When calculating the Mössbauer diffraction spectrum the amplitude of radiation scattered from a crystal (4.1) must be squared modulo and averaged over the source spectrum $\varepsilon(E - E_s)$ as well as over the angles of incidence:

$$S(E_s, \Delta\theta) \propto \sum_{s=\pi,\sigma} \int_{-\infty}^{\infty} dE\, \varepsilon(E - E_s) \int_{\alpha_1}^{\alpha_2} \frac{d\alpha}{2\sin(2\theta_B)} |R^s(E, \alpha)|^2 \tag{4.4}$$

$$\alpha_{1,2} = -2(\Delta\theta \pm 3'') \sin(2\theta_B).$$

The source spectrum $\varepsilon(E - E_s)$ was assumed to contain a single Lorentzian line with maximum at E_s and width $\Gamma_s = 2.5\Gamma_0$. The angular integration was performed in the $\pm 3''$ interval around each point $\Delta\theta = \theta - \theta_B$ displayed in figure 3(*a*). The angular range $\pm 3''$ took into account the incident beam divergence (4″) and the crystal bending (2″). Some results of the comparison of calculated and experimental spectra are shown in figures 3–5 (the calculated spectra were summed up over the same angular points as the experimental ones). In all cases the experimental dependences are fitted quite well by the calculated curves. From that, one can conclude that the Mössbauer spectra detected in the Bragg range have a shape essentially different from the Lorentzian one as the theory predicts.

4.2. Time dependence of the nuclear coherent response

To calculate the time evolution of coherent nuclear resonant scattering, the formalism of response functions [9, 10] was used. The calculations were performed for the idealised case of stepwise excitation only. The time evolution in the case considered is given by the expression derived in [29]:

$$T(t, \Delta\theta) \propto 2\,\mathrm{Re}\left(\sum_{s=\pi,\sigma} \int_0^t dt'\, G^s(t', \alpha) \cdot H^{s*}(t', \alpha) \right). \tag{4.5}$$

Here

$$G^s(t, \alpha) = \int \frac{dE}{2\pi\hbar} R^s(E, \alpha)\, e^{-iEt/\hbar} \tag{4.6}$$

and

$$H^s(t, \alpha) = i \int \frac{dE}{2\pi} \frac{R^s(E, \alpha)\, e^{-iEt/\hbar}}{E - E_s + i\Gamma_s/2} \tag{4.7}$$

where $G^s(t, \alpha)$ is the response function [9, 10]. $|G^s(t, \alpha)|^2$ shows the time dependence of

gamma-radiation emission at decay of the state excited by a very short pulse. When deriving equation (4.5) in [29] the source spectral distribution was taken into account and the gamma-radiation flux was assumed to be uncovered instantaneously. From (4.1) and (4.6) it is seen that $G^s(t, \alpha)$ has no longer simple exponential dependence as in the case of an isolated nucleus [29].

In the case when the electronic scattering gives a contribution to the diffraction along with the nuclear resonant one, the value $R^s(\infty, \alpha) \neq 0$. Since the part of $R^s(E, \alpha)$ related to electronic scattering does not depend on energy, it is convenient to separate it out:

$$\begin{aligned} R^s(E, \alpha) &= \tilde{R}^s(E, \alpha) + R^s(\infty, \alpha) \\ \tilde{R}^s(\infty, \alpha) &= 0. \end{aligned} \tag{4.8}$$

In view of equation (4.8) the general expression (4.5) takes the following form:

$$T(t, \Delta\theta) \sim \sum_{s=\pi,\sigma} |R^s(\infty, \alpha)|^2 \theta(t) + 2\,\mathrm{Re}\Big(\sum_{s=\pi,\sigma} \int_0^t \tilde{G}^s(t', \alpha)[\tilde{H}^{s*}(t', \alpha) + R^{s*}(\infty, \alpha) \exp(\mathrm{i}E_s t'/\hbar - \Gamma_s t/2\hbar)]\, \mathrm{d}t' \Big). \tag{4.9}$$

$\theta(t)$ is a unit stepwise function. The values $G^s(t, \alpha)$ and $H^s(t, \alpha)$ were calculated numerically. It should be noted that only one term with $l = 2$ (transition $\Delta m = 0$) was taken into account in sum (4.2). The contribution of neighbouring resonances could be neglected because of the large distance between them. It will be recalled also that this transition was excited by the π-polarised radiation component only.

The averaging of the time evolution of the coherent response over the angles of incidence was performed in a way similar to that used in calculations of the Mössbauer diffraction spectra.

An example of the comparison of computed and measured time dependences of diffraction $T(t, \Delta\theta)$ is given in figure 3(b). The experimental dependences are fitted fairly well by the calculated curves. The full curve in figure 3(a) represents the angular dependence of scattered radiation which was obtained from $T(t, \Delta\theta)$ at any time t, when the steady-state diffraction regime was achieved.

Using the calculated time and frequency dependences $T(t, \Delta\theta)$ and $S(E_s, \Delta\theta)$ averaged over the $\pm 3''$ intervals, the theoretical functions $\tau^*_{ex}(\theta - \theta_B)$, $\Gamma_{ex}(\theta - \theta_B)$ and $E_{ex}(\theta - \theta_B) - E_{02}$ were obtained and plotted in figure 5. The broken curves in these figures show similar functions calculated for an incident plane wave of gamma radiation.

One should point out in conclusion that all calculated time and frequency characteristics of collective nuclear excitations are in good agreement with the corresponding experimental values.

5. Discussion of gamma-exciton properties

5.1. Radiative corrections and the role of self-absorption

As is well known [30, 31], the energy of a nuclear excited state (as well as of an atom) changes due to interaction with a field of virtual photons and becomes equal to $E_0 = \tilde{E}_0 + \delta E$. The radiative self-energy δE is added to the self-energy $\tilde{E}_0$ of inter-nucleon interaction in a nucleus. Along with this, the energy level of a nuclear excited state is smeared, so that the energy distribution in the excited state acquires Lorentzian shape with width Γ_1. The Lorentzian distribution corresponds to the exponential law of de-excitation with characteristic radiative lifetime $\tau_1 = \hbar/\Gamma_1$. Together with the radiative

decay channel there exists a channel of internal conversion caused by the interaction of a nucleus with its electronic shell. This gives additional broadening of the level, Γ_2. Hence, the total width is equal to $\Gamma_0 = \Gamma_1 + \Gamma_2$, and the characteristic nuclear lifetime $\tau_0 = \hbar/\Gamma_0$.

The excitation in a system of identical nuclei, produced by a single resonant gamma photon, is non-localised: it spreads over the entire system. Radiative corrections to this collective excited state can be quite different from those in the case of isolated excitation. These corrections change drastically in coherent conditions. The new radiative corrections should result in new values for the lifetime of a collective excited state, for its energy width and for its excitation energy.

The radiative corrections are not always seen directly in the observed Mossbauer spectra and time dependences. For one- and two-dimensional nuclear systems any change in the linewidth and characteristic emission time is attributed to the radiative corrections only [5]. But for three-dimensional system it is not the case since the effect of resonant self-absorption plays some part and causes distortion of Lorentzian energy dependence and exponential de-excitation law (see Appendix). For that reason the true data concerning the energy and time parameters of excitations in bulk media are concealed.

In order to reveal factors influencing the spectral and time dependences of collective nuclear excitations in bulk media, let us consider some simplified theoretical models as an approach to the real situation.

5.2. *Gamma-exciton parameters in a pure nuclear matrix*

Let us assume that only the nuclear subsystem of a crystal interacts with gamma radiation. We shall also suppose the hyperfine splitting to be absent. In this case

$$\chi^{s}_{km} = 0$$
$$g^{s}_{km} = -g_0 \frac{\Gamma_0/2}{E - E_0 + i\Gamma_0/2}. \tag{5.1}$$

Let us calculate first of all the energy position of maximum reflectivity. We shall assign to it the meaning of the gamma-exciton energy.

5.2.1. Gamma-exciton energy. Let us introduce the dimensionless parameter $\Omega = (E - E_0)/\Gamma_0 + g_0/\alpha$. Substituting (5.1) into (4.1) one obtains after simple transformations

$$R(\Omega, \alpha) = -\frac{g_0}{\alpha(\Omega + i/2) \pm [(\Omega + i/2)^2\alpha^2 - g_0^2]^{1/2}}. \tag{5.2}$$

It is seen from (5.2) that the coherent scattering amplitude $R(\Omega, \alpha)$ satisfies the relation:

$$R(\Omega, \alpha) = -R^*(-\Omega, \alpha). \tag{5.3}$$

Hence, it appears that the diffraction spectrum in a three-dimensional nuclear crystal lattice, $S(\Omega, \alpha)$, which is equal to $|R(\Omega, \alpha)|^2$, is symmetrical about the point $\Omega = 0$. One can easily show that the centre of symmetry $\Omega = 0$ corresponds to the maximum of an excitation spectrum. Thus, for radiation incident upon a nuclear crystal near the Bragg angle, the maximum reflectivity is reached at the energy

$$E_{ex}(\alpha) = E_0 - \Gamma_0 g_0/\alpha. \tag{5.4}$$

At large deviations from the Bragg angle when $|\alpha| \gg g_0$, the E_{ex} value approaches the

resonant energy of an isolated nucleus, E_0. At the same time, it can be seen from (5.2) that the scattering amplitude in this limiting case acquires the ordinary resonance energy dependence $\sim(E - E_0 + i\Gamma_0/2)^{-1}$. However, near the Bragg point the deviation of E_{ex} from E_0 is large and varies inversely with α while having the same sign as $\Delta\theta$.

It is interesting to note that at the energy $E = E_{ex}$, when $\Omega = 0$, the scattering amplitude $R(0, \alpha)$, equation (5.2), has a purely imaginary value just as in the case of scattering from an ordinary resonance:

$$R(0, \alpha) = i\frac{g_0}{\alpha/2 \pm (\alpha^2/4 + g_0^2)^{1/2}} = ir(\alpha). \tag{5.5}$$

At the exact Bragg angle position $\alpha = 0$ the energy dependence in (5.2) disappears. Also the whole energy incident on a crystal is reflected elastically without losses $|R(\Omega, 0)|^2 = 1$, despite the existence of a strong inelastic channel in scattering from an isolated nucleus. The latter effect is a manifestation of the suppression of inelastic channels in a nuclear reaction [4, 6, 27].

5.2.2. Gamma-exciton energy width. Let us consider now the dependence of collective nuclear resonance width on the angle of incidence of gamma radiation on a crystal. The condition for determination of the resonance width Γ_{ex} at half-maximum of the energy peak is written in the following form:

$$\begin{aligned} &\Gamma_{ex} = 2\Gamma_0|\Delta\Omega| \\ &R(\Delta\Omega, \alpha) = ir(\alpha)\, e^{i\varphi}/\sqrt{2}. \end{aligned} \tag{5.6}$$

Here φ is the unknown phase, and $r(\alpha)$ was determined in (5.5). Solving equation (5.6) one obtains

$$\begin{aligned} 2\Delta\Omega &= (g_0/\alpha)\frac{2 + r^2(\alpha)}{\sqrt{2}r(\alpha)}\sin\varphi \\ \cos\varphi &= (\alpha/g_0)\frac{\sqrt{2}r(\alpha)}{2 - r^2(\alpha)}. \end{aligned} \tag{5.7}$$

Let us consider again two limiting cases. Close to the Bragg angle, when $|\alpha/g_0| \ll 1$, one gets the following expression for Γ_{ex}:

$$\Gamma_{ex}(\alpha) = \frac{3}{\sqrt{2}}\Gamma_0 g_0/|\alpha| \tag{5.8}$$

i.e. the collective nuclear resonance width tends to infinity when approaching the Bragg angle. At a large distance from θ_B, when $|\alpha/g_0| \gg 1$, the collective nuclear resonance width Γ_{ex} tends to the natural width of an isolated nucleus Γ_0:

$$\Gamma_{ex}(\alpha) = \Gamma_0(1 + g_0^2/2\alpha^2). \tag{5.9}$$

5.2.3. Gamma-exciton time characteristics. To simplify calculations let us determine the value τ_{ex}, the characteristic emission time at spontaneous decay of some definite gamma-exciton mode, rather than the response time τ_{ex}^* measured in the experiment. We shall assume that the nuclear system was excited by a short radiation pulse. In this case the time dependence of emission in the Bragg angle direction is proportional to $|G(t, \alpha)|^2$ [10]. For a pure nuclear diffraction the function $G(t, \alpha)$ is equal to [10]

$$\begin{aligned} G(t, \alpha) &= i\exp(-iE_0 t/\hbar - t/2\tau_0)\frac{J_1(\eta t/\tau_0)}{t}\exp(i\eta t/\tau_0)\theta(t) \\ \eta &= g_0/(\alpha - 2\chi_{00}). \end{aligned} \tag{5.10}$$

J_1 is the Bessel function of the first order. Under the condition $\chi_{00} = 0$ one obtains the following formula for the time dependence of emission at coherent de-excitation:

$$T(t, \alpha)/T(0, \alpha) = \frac{J_1^2(tg_0/\alpha\tau_0)}{(tg_0/2\alpha\tau_0)^2} \exp(-t/\tau_0)\theta(t). \tag{5.11}$$

At small deviations from the Bragg angle, when $|\alpha/g_0| \ll 1$, the exponent in (5.11) can be omitted. Then the characteristic emission time at the gamma-exciton decay is equal to

$$\tau_{ex}(\alpha) = 1.91\tau_0|\alpha|/g_0 \tag{5.12}$$

i.e. the characteristic time tends to zero linearly when approaching the Bragg angle. At a large distance from θ_B, when $|\alpha/g_0| \gg 1$, the exponential function makes the principal contribution. Then

$$\tau_{ex}(\alpha) = \tau_0(1 - g_0^2/4\alpha^2). \tag{5.13}$$

One should note that in both limiting cases the relation

$$\tau_{ex}(\alpha)\Gamma_{ex}(\alpha) \sim \tau_0\Gamma_0 = \hbar \tag{5.14}$$

holds, which represents the energy–time uncertainty relation.

5.3. Gamma-exciton parameters with an account of electronic scattering

In the previous section the gamma-exciton parameters were calculated within the framework of a model that took into account the interaction of gamma radiation with the nuclear system only. The interaction with electrons was neglected. This approximation outlines qualitatively the resonance broadening and the decay speed-up observed in the experiment. But it does not describe the details of experimental dependences obtained. First, the calculated gamma-exciton parameters E_{ex}, Γ_{ex} and τ_{ex} are not constrained at the exact Bragg position. Secondly, the approximation mentioned does not describe the gamma-exciton spectral asymmetry (figure 4).

Let us consider a further approximation that takes electronic scattering into account. We shall conserve the pure nuclear diffraction conditions, i.e. coherent scattering at non-zero angles proceeds, as before, due to the nuclear resonant interaction only. But at the same time the coherent electronic scattering in the forward direction will be taken into account. It means now that $\chi_{00} \neq 0$. The expression for the coherent scattering amplitude, obtained within the framework of this model, is similar to (5.2), but with substitution of α by $\tilde{\alpha} + 2i\chi''_{00}$, where $\tilde{\alpha} = \alpha - 2\chi'_{00}$. The real part χ'_{00} gives rise to a small angular shift of the Bragg peak only. The influence of the imaginary part on time and frequency properties of collective nuclear excitations is more substantial. For example, one can easily show that, by introducing the non-zero value of χ''_{00}, expression (5.4), which defines the energy position of the reflection intensity maximum, acquires a new form:

$$E_{ex}(\tilde{\alpha}) = E_0 - \Gamma_0 \frac{\tilde{\alpha}g_0}{\tilde{\alpha}^2 + 4g_0\chi''_{00}}. \tag{5.15}$$

The validity of equation (5.15) is limited by the requirement that is usually implemented in the experiment, namely, $2\chi''_{00} \ll g_0$. As follows from (5.15), the maximum deviation from an isolated-nucleus resonance is reached at a distance $\tilde{\alpha}^* = \pm 2(g_0\chi''_{00})^{1/2}$ off the Bragg position. The maximum deviation itself is equal to $E_{ex} = \pm 0.25\Gamma_0(g_0\chi''_{00})^{1/2}$. Thus, there is no longer divergence at $\tilde{\alpha} = 0$ and equation (5.15) describes qualitatively the experimental dependence in figure 5(*c*).

The account of χ''_{00} means physically that the photo-electric absorption by atoms is included into consideration. Within the framework of the model considered earlier in § 5.2, the incident radiation in the close neighbourhood of the Bragg angle could penetrate infinitely into the crystal. The penetration depth is proportional to $\lambda(2|\alpha|g_0)^{-1/2}$ [27] in that case. But now the penetration is limited by electronic absorption and does not exceed a value proportional to λ/χ''_{00}. The estimations show that for this reason the expressions obtained for gamma-exciton parameters in § 5.2 appeared to be inaccurate in the angular range $|\tilde{\alpha}| \leqslant (g_0\chi''_{00})^{1/2}$. At the same time for $|\tilde{\alpha}| > (g_0\chi''_{00})^{1/2}$ where the depth of the coherent nuclear resonant interaction is smaller than the photo-electric absorption depth, all conclusions of the previous section are valid.

The limitation imposed by electronic absorption on the coherent nuclear resonant interaction volume also inhibits the infinite growth of the collective nuclear resonance width at the exact Bragg position. One can show by a method similar to that employed in § 5.2.2 that, in the presence of electronic absorption, the gamma-exciton resonance width reaches its maximum value at $\tilde{\alpha} = 0$. In particular, in the case $\beta = (2\chi''_{00}/g_0)^{1/2} \ll 1$, which is usually implemented in the experiment, it is equal to

$$\Gamma_{ex}(0) = \Gamma_0 \nu \frac{g_0}{2\chi''_{00}}$$
$$\nu = \frac{1 + 3\beta}{3\sqrt{2}}(1 + 16\beta/3)^{1/2}. \tag{5.16}$$

At the same angular point $\tilde{\alpha} = 0$ the characteristic emission time τ_{ex} reaches its minimal value. To calculate $\tau_{ex}(0)$ we shall use expression (5.10). In view of this expression, the time evolution of emission from a nuclear system, excited at the Bragg angle, takes the form

$$T(t, \tilde{\alpha} = 0) \propto \exp[-t(\tau_0^{-1} + 2\tau_B^{-1})] \frac{I_1^2(t/\tau_B)}{t^2}\theta(t)$$
$$\tau_B = \tau_0 2\chi''_{00}/g_0. \tag{5.17}$$

Here $I_n(x)$ is the nth-order Bessel, function of imaginary argument. As follows from (5.17), the characteristic emission time is

$$\tau_{ex}(0) = 1.09\tau_0\chi''_{00}/g_0. \tag{5.18}$$

It is seen that the limitation, imposed by photo-electric absorption on the volume of coherent nuclear interaction, substantially influences collective nuclear excitation parameters.

The inclusion of χ''_{00} changes not only the resonant parameters but also the shape of the collective excitation spectrum. Equation (5.3), which describes the gamma-exciton spectrum symmetry in a pure nuclear crystal matrix, is violated immediately when χ''_{00} takes a non-zero value, i.e. as soon as the photo-electric absorption of radiation is considered. There exists a single angular position $\tilde{\alpha} = 0$ when the symmetry is restored. When passing through it, the asymmetry changes sign.

5.4. Gamma-exciton parameters in the induced Borrmann effect conditions

The approximation considered above and the formulae obtained relate to the so-called case of pure nuclear magnetic reflection, when the Rayleigh scattering amplitude is suppressed within each group of atoms of the same type. In the experiment considered

a nearly pure nuclear reflection was used, which is implemented in a different way—due to accidental cancellation of the Rayleigh scattering amplitude within a unit cell [15]. In this case the wave fields inside a crystal are built up by the nuclear diffraction in such a way that, along with low nuclear absorption, these fields also undergo anomalously low electronic absorption. As a result the Borrmann effect is induced [24, 32] together with the suppression effect. For this reason close to the Bragg angle $|\alpha| < 2\chi''_{01}$, the radiation penetrates into the crystal deeper than in the case of magnetic pure nuclear diffraction (but still not as deep as in the case of pure nuclear matrix—§ 5.2). Hence, the region of coherent nuclear resonant interaction increases. This means that our experimental case is positioned between the models considered in § § 5.2 and 5.3. The collective resonance width $\Gamma_{ex}(0)$ increases as compared to (5.16), and the emission time $\tau_{ex}(0)$ decreases as compared to (5.18). In this case the maximum deviation of collective nuclear resonance energy $E_{ex} - E_0$ turns out to be larger than that calculated by formula (5.15), and the angle at which it is reached is smaller. The calculated dependences corresponding to this approximation are shown in figure 5 by the broken curves.

Thus, the consideration of various models shows that the interaction of radiation with an electronic system in the angular range near the Bragg position controls the volume of a nuclear system responding coherently to the excitation and, hence, significantly affects the gamma-exciton parameters.

6. Conclusions

Collective nuclear excitations play an important part in the resonant scattering of gamma radiation in a perfect crystal. The significant role of collective excitations is due to a strong time and space correlation between excitation phases in a system containing a macroscopic number of regularly arranged nuclei. In the state of correlated resonant excitation, strong dynamic coupling is established between the radiation field and the nuclear matrix. In these conditions the wave field and the nuclei in a crystal are coupled into a unified physical state, which we refer to as a nuclear gamma exciton or in short a gamma exciton. Unlike the light exciton, which can be considered to be an analogue of a nuclear gamma exciton, one can neglect the direct interaction between the resonators, namely the nuclei. The coupling between nuclei is accomplished only indirectly—through the radiation field.

The investigations of gamma-exciton properties in the $^{57}FeBO_3$ crystal show that their characteristics, such as excitation energy, resonance width and lifetime, undergo considerable changes as the angle of incidence of the gamma radiation varies. The evolution of resonant parameters is attributed to changes in a radiative channel of interaction only. The 200-fold increase in nuclear resonance radiative width at the Bragg angle was observed. This implies that in our experiment the resonance radiative width is approximately 20 times greater than the inelastic conversion partial width. The increase of a gamma-exciton resonance width was accompanied by a corresponding drastic reduction of its lifetime.

Unfortunately, some interesting questions are beyond the scope of the present experimental investigations; for example, the properties of gamma excitons excited very far from the Bragg angle. In the off-Bragg angular range (this situation was considered theoretically in [5, 33]) the course of variation of the resonant properties of a gamma exciton is reversed compared to those of an isolated nucleus: the resonance narrows and the decay slows down. Far from the Bragg angle the partial radiative width can disappear

completely. Since the conversion dominates at low-energy nuclear resonances, the disappearance of the radiative width and, hence, the slowing down of the nuclear excited state decay are effects that can hardly be observed. So far the narrowing of elastic width was detected only indirectly in [34].

Acknowledgments

The authors would like to express their gratitude to K P Aleshin, M A Volkov, A S Subbotin and I B Filippov for technical assistance in the preparation of the experiment. We acknowledge also Professor Yu M Kagan, Professor V G Kohn, Dr U van Burck, Dr A I Chumakov, M V Zelepukhin and S L Popov for useful discussions and valuable remarks.

Appendix

The amplitude of elastic resonant scattering from the quasi-discrete level of a nucleus has the form

$$R_0(E) = -\frac{1}{2\kappa}\frac{\Gamma_0}{E - E_0 + i\Gamma_0/2}. \tag{A1}$$

Here κ is the radiation wavenumber.

The time dependence of emission during the decay of a nuclear excited state is defined by the response function $G_0(t)$, which is the Fourier transform of (A1):

$$G_0(t) = i\frac{1}{2\kappa\tau_0}\exp(-iE_0t/\hbar - t/2\tau_0)\theta(t). \tag{A2}$$

It was shown in [10] that the time dependence of emission for spontaneous decay following excitation by a very short radiation pulse is proportional to $|G_0(t)|^2$.

As a rule, the time evolution of decay and the evolution of emission of decay products are identified. However, if a decaying nucleus is situated in the bulk medium containing resonant nuclei, then the time dependence of emission of decay products is distorted compared to the time dependence of a nuclear decay itself. The physical reason for this is the resonant self-absorption of gamma-radiation in the medium.

Let us consider the simple case of incoherent resonant scattering from nuclei filling the space on one side of some arbitrary plane. The radiation is incident at angle $\pi/2 - \theta_1$ onto this plane. The detector records radiation emitted at angle $\pi/2 - \theta_2$. If the scattering took place from a nucleus located at depth z below the surface, then the scattering amplitude can be written in the following form:

$$\begin{aligned} R_0'(E, z) &= \exp\left(i\frac{\kappa z}{2\gamma_1}n(E)\right)R_0(E)\exp\left(i\frac{\kappa z}{2\gamma_2}n(E)\right) \\ n(E) &= 1 + \frac{N}{2\kappa}\left(-\sigma_r\frac{\Gamma_0/2}{E - E_0 + i\Gamma_0/2} + i\sigma_{ph}\right) \\ \gamma_1 &= \cos\theta_1 \qquad \gamma_2 = \cos\theta_2. \end{aligned} \tag{A3}$$

Here $n(E)$ is the complex refractive index, the imaginary part of which describes absorption in matter; σ_r and σ_{ph} are the cross sections of resonant and photo-electric absorption,

respectively; and N is the number of resonant nuclei in unit volume. When deriving (A3) it was assumed that electronic scattering from atoms can be neglected. But the photo-electric absorption should be considered, since it determines the maximally possible penetration depth of radiation inside a medium. If the matter contains atoms with non-resonant nuclei, then their photo-absorption must also be taken into account in (A3).

In the case under consideration the response function can be calculated analytically by using definition (4.6) as well as (A3):

$$G_0'(t, z) \propto \exp(-E_0 t/\hbar - t/2\tau_0) J_0(2(\mu_r t z/2\tau_0)^{1/2}) \exp(-\mu_{ph} z/2)\theta(t)$$
$$\mu_r = \sigma_r N \qquad \mu_{ph} = \sigma_{ph} N \tag{A4}$$

where $J_n(x)$ is the Bessel function of nth order.

To calculate the time dependence of gamma-radiation emission from the target, the contributions of all nuclei should be summed up. For this purpose the value $|G_0'(t, z)|^2$ should be integrated over z. We shall get as a result that the intensity of emission following the excitation of a target by a short pulse behaves in time as

$$T_0'(t) \sim \exp[-t(\tau_0^{-1} + \tau_A^{-1})] I_0(t/\tau_A)\theta(t)$$
$$\tau_A = \tau_0 2\sigma_{ph}/\sigma_r. \tag{A5}$$

(It should be noted that the characteristic time parameters τ_A in (A5) and τ_B in (5.17) are identical if coherent and incoherent scattering are considered in the same substance, the single crystal for example.)

Let us assume that the resonant absorption considerably exceeds the photo-electric one, i.e. $\sigma_r \gg \sigma_{ph}$. Then $\tau_0 \gg \tau_A$.

In the limiting cases, equation (A5) is simplified. For example, for $t < \tau_A$

$$T_0'(t) \sim \exp(-t/\tau_A)\theta(t) \tag{A6}$$

and for $t \gg \tau_A$

$$T_0'(t) \sim \frac{\exp(-t/\tau_0)}{(t/\tau_A)^{1/2}}\theta(t). \tag{A7}$$

As is seen that due to resonance self absorption the emission of radiation from the bulk target proceeds according to a non-exponential law and considerably faster than an excited nucleus decay. It is of interest to compare the time evolution of incoherent emission from the bulk target with the coherent one.

As follows from (5.17), the time evolution of coherent emission from a nuclear system, excited at the Bragg angle is described by a function that resembles (A5). In particular, immediately after excitation, both dependences have an exponential dependence in time. Really, for $t < \tau_B$ equation (5.17) takes the form

$$T(t, \tilde{\alpha} = 0) \sim \exp(-2t/\tau_B)\theta(t). \tag{A8}$$

On the other hand, in the time interval $t \gg \tau_B$ the dependences are essentially different. The coherent emission proceeds faster and follows the law [9, 10]

$$T(t, \tilde{\alpha} = 0) \propto \frac{\exp(-t/\tau_0)}{t^3}\theta(t). \tag{A9}$$

Thus, it is seen that in both cases the emission of gamma radiation from the bulk target is speeded up, compared to the time dependence of an isolated nucleus decay. The physical reasons leading to the emission speed-up are quite different, however.

References

[1] Dicke R H 1954 *Phys. Rev.* **93** 99
[2] Trammell G T 1961 *Chemical Effects of Nuclear Transformations* vol. 1 (Vienna: IAEA) p 75
[3] Afanas'ev A M and Kagan Yu 1965 *Pis. Zh. Eksp. Teor. Fiz.* **2** 130 (1965 *JETP Lett.* **2** 81)
[4] Afanas'ev A M and Kagan Yu 1965 *Zh. Eksp. Teor. Fiz.* **48** 327 (1965 *Sov. Phys.–JETP* **21** 215)
[5] Kagan Yu and Afanas'ev A M 1966 *Zh. Eksp. Teor. Fiz.* **50** 271 (1966 *Sov. Phys.–JETP* **23** 188)
[6] Kagan Yu, Afanas'ev A M and Perstnev I P 1968 *Zh. Eksp. Teor. Fiz.* **54** 1530 (1968 *Sov. Phys.–JETP* **27** 819)
[7] Hannon J P and Trammell G T 1968 *Phys. Rev.* **169** 315
[8] Hannon J P and Trammell G T 1969 *Phys. Rev.* **186** 306
[9] Kagan Yu, Afanas'ev A M and Kohn V G 1978 *Phys. Lett.* **68A** 339
[10] Kagan Yu, Afanas'ev A M and Kohn V G 1979 *J. Phys. C: Solid State Phys.* **12** 615
[11] Davydov A S 1976 *Solid Stte Physics* (Moscow: Nauka) (in Russian) p 349
[12] Zaretskii D F and Lomonosov V V 1965 *Zh. Eksp. Teor. Fiz.* **48** 368 (1965 *Sov. Phys.–JETP* **21** 243)
[13] Debrunner P and Morrison R J 1965 *Rev. Sci. Instrum.* **36** 145
[14] Thieberger P, Moragues J A and Sunyar A W 1968 *Phys. Rev.* **171** 425
[15] van Bürck U, Smirnov G V, Mossbauer R L, Maurus H J and Semioschkina N A 1980 *J. Phys. C: Solid State Phys.* **13** 4511
[16] Chechin A I, Andronova N V, Zelepukhin M V, Artem'ev N A and Stepanov E P 1983 *Pis. Zh. Eksp. Teor. Fiz.* **37** 531 (1983 *JETP Lett.* **37** 633)
[17] Smirnov G V, Shvyd'ko Yu V and Realo E 1984 *Pis. Zh. Eksp. Teor. Fiz.* **39** 33 (1984 *JETP Lett.* **39** 41)
[18] Smirnov G V, Shvyd'ko Yu V, Kolotov O S, Pogozhev V A, Kotrbova M, Kadechkova S and Novak J 1984 *Zh. Eksp. Teor. Fiz.* **86** 1495 (1984 *Sov. Phys–JETP* **59** 875)
[19] Smirnov G V and Shvyd'ko Yu V 1986 *Pis. Zh. Eksp. Teor. Fiz.* **44** 431 (1986 *JETP Lett.* **44** 556)
[20] van Bürck U, Mössbauer R L, Gerdau E, Rüffer R, Hollatz R, Smirnov G V and Hannon J P 1987 *Phys. Rev. Lett.* **59** 355
[21] Fagel G, Siddons D P, Hastings J R, Houstein P E, Grover G R and Berman L E 1988 *Phys. Rev. Lett.* **61** 2797
[22] Kolotov O S, Pogozhev V A, Smirnov G V and Shvyd'ko Yu V 1987 *Fiz. Tverd. Tela* (Leningrad) **29** 2548 (1987 *Sov. Phys.–Solid State* **29** 1471)
[23] Kotrbova M, Kadechkova S, Novak J, Bradler J, Smirnov G V and Shvyd'ko Yu V 1985 *J. Cryst. Growth* **71** 607
[24] Smirnov G V, Shvyd'ko Yu V, van Bürck U and Mössbauer R L 1986 *Phys. Status Solidi* b **134** 465
[25] Diehl D, Jantz W, Nolang B I and Wettling W 1984 *Curr. Topics Mater. Sci.* **11** 241
[26] Eibschutz M and Lines M E 1973 *Phys. Rev.* B **7** 4907
[27] Maurus H J, van Bürck U, Smirnov G V and Mössbauer R L 1984 *J. Phys. C: Solid State Phys.* **17** 1991
[28] Smirnov G V and Chumakov A I 1985 *Zh. Eksp. Teor. Fiz.* **89** 1169 (1985 *Sov. Phys.–JETP* **62** 673)
[29] Smirnov G V and Shvyd'ko Yu V 1989 *Zh. Eksp. Teor. Fiz.* **95** 777 (1989 *Sov. Phys. JETP* **68** 444)
[30] Heitler W 1954 *Quantum Theory of Radiation* (London: Oxford University Press)
[31] Akhiezer A I and Berestetskii V D 1969 *Quantum Electrodynamics* (Moscow: Nauka) (in Russian)
[32] van Bürck U, Maurus H J, Smirnov G V and Mössbauer R L 1984 *J. Phys. C: Solid State Phys.* **17** 2003
[33] Afanas'ev A M and Kagan Yu 1967 *Zh. Eksp. Teor. Fiz.* **52** 191 (1967 *Sov. Phys.–JETP* **25** 124)
[34] Smirnov G V and Shvyd'ko Yu V 1982 *Pis. Zh. Eksp. Teor. Fiz.* **35** 409 (1982 *JETP Lett.* **35** 505)